Assessing Potential Links between Climate Variability and Mean and Extreme Surface Temperatures throughout the United States

Jason Giovannettone *

Posted Date: 21 June 2023

doi: 10.20944/preprints202306.1546.v1

Keywords: climate variability; climate indices; low-frequency oscillations; temperature; ENSO; heat waves; Western Hemisphere Warm Pool

Article

Assessing potential links between climate variability and mean and extreme surface temperatures throughout the United States

Jason Giovannettone [1,*]

[1] Sisters of Mercy of the Americas, Silver Spring, MD, USA; jgiovannettone@sistersofmercy.org

* Correspondence: jgiovannettone@sistersofmercy.org; Tel.: +16125546159

Abstract: In order to better understand the extent to which global climate variability is linked to the frequency and intensity of heat waves and overall changes in temperature throughout the United States (US), correlations between long-term monthly mean, minimum, and maximum temperatures measured at sites throughout the contiguous US and low-frequency variability of multiple climate indices (CIs) are analyzed over the period 1948 to 2018 using correlation analysis. The Pearson's correlation coefficient is used to assess correlation strength, while Leave-One-Out Cross-Validation and a bootstrapping technique (p-value) are used to address potential serial and spurious correlation and assess the significance of each correlation. Three parameters defined the sliding windows over which surface temperature and CI values were averaged: window size, lag time between the temperature and CI windows, and the beginning month of the temperature window. A 60-month sliding window size and 0 lag time resulted in the strongest correlations overall; beginning months were optimized on an individual site basis. Strong ($r >= 0.60$) and significant (p-value <= 0.05) correlations were identified. The Western Hemisphere Warm Pool (WHWP) and El Niño/Southern Oscillation (ENSO) exhibited the strongest links to temperatures in the western US, tropical Atlantic sea surface temperatures to temperatures in the central US, the WHWP to temperatures throughout much of the eastern US, and atmospheric patterns over the northern Atlantic to temperatures in the Northeast and Southeast. The final results were compared to results from previous studies focused on precipitation and coastal sea levels. Regional consistency was found regarding links between the northern Atlantic and overall weather and coastal sea levels in the Northeast and Southeast as well as on weather in the upper Midwest. Though the MJO and WHWP revealed dominant links with precipitation and temperature, respectively, throughout the West, ENSO revealed consistent links to sea levels and surface temperatures along the West Coast. These results help focus future research regarding specific mechanisms of climate variability that appear the exhibit strong links to US regional weather and sea level variability and prediction.

Keywords: climate variability; climate indices; low-frequency oscillations; temperature; ENSO; heat waves; Western Hemisphere Warm Pool

1. Introduction

The most visible weather/climate trend that can be verifiably attributed to climate change is the persistent increase in global temperatures since the late 1700's to early 1800's. The Intergovernmental Panel on Climate Change (IPCC) regarded this causality as *likely* with *very high confidence* [1]. More recently, global temperatures have experienced a sudden acceleration over the last 50 years, resulting in overall rate of temperature rise that is unprecedented when compared to the previous 2000 years [1]. Mean global surface temperature in the most recent decade of 2011-2020 has increased by 0.95 to 1.20°C compared to 1850-1900 and is *very likely* projected to rise further up to a total increase of 1.3 to 2.4°C for the period of 2081-2100 when considering an intermediate-low emissions scenario (i.e., Shared Socio-economic Pathway 1 (SSP1)-2.6) [1].

Preprints (www.preprints.org) | NOT PEER-REVIEWED | Posted: 21 June 2023 doi:10.20944/preprints202306.1546.v1

Projected increases in annual mean surface temperature are not consistent globally or even within a particular country. For example, long-term (i.e., 2081-2100) increases of 2.0 to 3.0°C compared to the recent past (i.e., 1995-2014) are projected in the Midwest and Northeast regions of the United States (US) based on the Coupled Model Intercomparison Project Phase 6 (CMIP6) model simulations using the SSP1-2.6 emissions scenario, while a less extreme increase of 1.0 to 2.0°C is projected for the remainder of the US under the same scenario [2]. Lee et al. [2] also show that the projected rise throughout the US in the mid- and long-term scenarios using the higher intermediate-high (i.e., SSP3-7.0) emissions scenario is more highly dependent on proximity to the ocean. For example, consistent with past trends in land vs. ocean surface temperatures, temperatures throughout the entire interior of the US are projected under SSP3-7.0 to increase by a maximum of 3.0°C for the period 2041-2060 relative to the recent past, while areas closer to the coasts are expected to experience a maximum increase of 2.0°C.

In addition to the projected increases in the magnitude of mean, as well as extreme, temperatures, the changing persistence of temperature extremes (i.e., heat waves) is of grave concern. Perkins [3] describes heat waves as longer-than-normal periods of high temperatures that, in addition to wider contrasts between short-term and seasonal minimum and maximum temperatures, can significantly impact the natural and built environments (e.g., structural integrity of bridges and buildings and damage to pavements and railways) as well as have serious negative implications on human health and mortality [4]. Multiple studies have assessed past changes in the behavior of heat waves over the last several decades in the US [5] and globally [3, 6]. Regarding future projections, the effects of climate change on heat waves will likely be more severe in urban areas due to the "urban heat island" effect. Zhang and Ayyub [7], for example, projected that the magnitude of heat waves being experienced in Washington, DC, will increase by about 5.7°C by 2100 using the high emissions greenhouse gas emissions scenario or representative concentration pathway (RCP) RCP8.5; the authors also estimated that the frequency and duration of said heat waves will double in the same time frame. Vose et al. [8] also support projections of more intense heat waves in the future, but also projects a decrease in the intensity of cold extremes. In either case, an important aspect of extreme temperatures, whether hot or cold, is a clear understanding of the influence of climate variability.

As climate change in the form of an increase in global carbon emissions has a clear effect on the increasing trend observed in mean ocean and global surface temperatures, extreme temperatures result from the added variance due to short-term climate variability superimposed on this trend, the basic mechanisms of which are still not well understood [9]. As ocean currents have a major influence on global weather, particularly regarding surface temperatures, the primary modes of climate variability considered in previous studies tend to focus on those that either directly characterize sea surface temperatures (SSTs) (e.g., the Atlantic Multidecadal Oscillation (AMO), the Caribbean index (CAR), and the Western Hemisphere Warm Pool (WHWP) or atmospheric processes that have a strong influence on SSTs (e.g., the El Niño/Southern Oscillation (ENSO), the North Atlantic Oscillation (NAO), and the Pacific Decadal Oscillation (PDO)).

ENSO is the leading mode of interannual SST variability throughout the tropical Pacific Ocean [10], and as such, has been found to have a significant impact on surface temperature variability in the US, particularly at the subseasonal time scale [11]. The specific mechanism by which ENSO affects US climate is through the generation of Rossby waves in the western subtropical North Pacific and the subsequent northward and then eastward propagation toward North America. ENSO's influence on the North Pacific jet stream, particularly during its warm phase (i.e., El Niño) when water located along the equator in the eastern Pacific becomes anomalously warm, causes it to strengthen and extend farther eastward than average; the opposite effect is observed during ENSO's cool phase (i.e., La Niña). Through the mechanisms mentioned above, ENSO has been found to influence sub-seasonal surface air temperatures within multiple regions in the US: La Niña has been associated with extended periods of colder than normal temperatures in the northwestern and north-central US [10, 12] during the winter months, while El Niño has been associated with warmer conditions over the Northeast during the winter and spring months and colder conditions over the Southeast during the autumn and winter months [13]. Various CIs that measure SSTs in different regions within the

Preprints (www.preprints.org) | NOT PEER-REVIEWED | Posted: 21 June 2023 doi:10.20944/preprints202306.1546.v1

equatorial eastern Pacific are used to characterize the current phase and strength of ENSO; these include the Multivariate ENSO Index (MEI) [14]; the Niño 1+2, 3, 3.4, and 4 regions; the Southern Oscillation Index (SOI) [15]; and the Trans-Niño Index (TNI) [16]. Refer to Figure 1 for approximate locations characterized by the ENSO as well as other CIs discussed.

Similar to ENSO, the PDO experiences two phases that are characterized by changes in SSTs and atmospheric pressure in the North Pacific and as well as along the Pacific Coast, though the time scales over which these phases occur are longer. Warm phases of the PDO are characterized by cooler SSTs in the Central North Pacific and warmer SSTs along the western coast of North America [17]. During the winter and spring months (i.e. November – April), warm phases of the PDO are typically associated with anomalously warm temperatures in northwestern North America and along the West Coast and anomalously cool temperatures in the southeastern US; the reverse pattern occurs during the negative phase.

An area of SSTs along the west coast of North America affected by ENSO and the PDO also includes a portion of what is referred to as the WHWP. The WHWP is the second largest region of very warm water on Earth defined by water temperatures greater than 28.5°C. It includes a small portion of the eastern North Pacific, the Gulf of Mexico, the Caribbean, and the western North Atlantic [18–19]. Due to its high temperatures, the WHWP represents a significant source of heat to the atmosphere, which can have a substantial effect on temperatures throughout the contiguous US. Due to the fact that the WHWP encompasses the entire Florida Current, which eventually feeds into the Gulf Stream, the WHWP can impact land temperature along the East Coast as well. In addition, a connection between the WHWP and ENSO through a "tropospheric bridge" has been found to facilitate warmer SSTs in the tropical North Atlantic and WHWP during an El Niño event [20]. In addition, the CAR [21], which represents average SST anomalies within the Caribbean and thus is entirely located within the WHWP, can provide additional details in terms of the potential influence of SSTs south of the US on US surface temperatures.

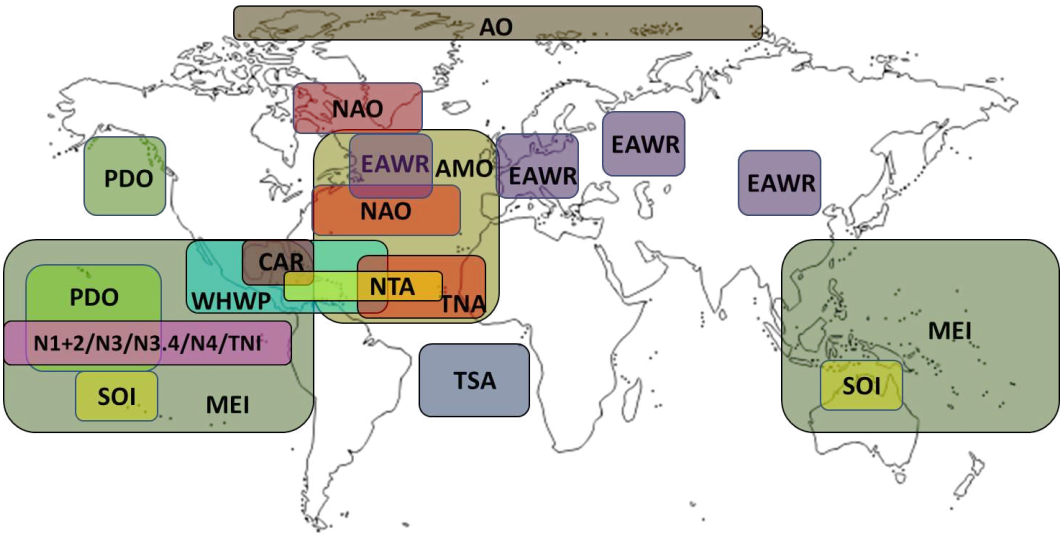

Figure 1. Locations characterized by various CIs in terms of SSTs and atmospheric behavior (i.e. pressure and height anomalies). The CIs indicated by each abbreviation are defined in Table 1.

Table 1. CIs (abbreviations and names) assessed along with their respective periods of record. Detailed definitions of each climate index can be found at NOAA [22].

CI (abb.)	Climate Index	Beginning Year	Ending Year
AO	Arctic Oscillation	1950	2018

Preprints (www.preprints.org) | NOT PEER-REVIEWED | Posted: 21 June 2023 doi:10.20944/preprints202306.1546.v1

AMO	Atlantic Multidecadal Oscillation	1948	2018
CAR	Caribbean Index	1950	2018
EAWR	Eastern Asia/Western Russia	1950	2013
MEI	Multivariate ENSO Index	1950	2018
N12	Niño 1+2	1950	2018
N3	Niño 3	1950	2018
N34	Niño 3.4	1950	2018
N4	Niño 4	1950	2018
NAO	North Atlantic Oscillation	1950	2018
NTA	North Tropical Atlantic index	1950	2018
PDO	Pacific Decadal Oscillation	1948	2018
SOI	Southern Oscillation Index	1951	2018
TNI	Trans-Niño Index	1948	2018
TNA	Tropical Northern Atlantic index	1948	2018
TSA	Tropical Southern Atlantic index	1948	2018
WHWP	Western Hemisphere Warm Pool	1948	2018

Overlapping a significant portion of the eastern half of the WHWP, there are two CIs that characterize SSTs over a large portion of the tropical North Atlantic while one CI additionally characterizes SSTs in the equatorial and tropical South Atlantic. The North Tropical Atlantic index (NTA) describes SSTs over the portion of the tropical North Atlantic extending from 6N to 18N between 60°W and 20°W and from 6°N to 10°N between 20°W and 10°W [21]. Overlapping the NTA and extending further east, the Tropical Northern Atlantic index (TNA) characterizes the anomalies of average monthly SSTs over the portion of the tropical North Atlantic extending from 5.5°N to 23.5°N/15°W to 57.5°W [23]. Further south, the Tropical Southern Atlantic index (TSA) characterizes SSTs from Equator to 20°S/10°E to 30°W [23]. The NTA and the TNA are especially important in any study of potential mechanisms by which temperatures within the US are modulated by SSTs due to a direct teleconnection between these CIs and ENSO. During the El Nino phase eastward-propagating equatorial Kelvin waves transport tropospheric temperature changes from over the eastern and central tropical Pacific to the tropical North Atlantic [24]; an eastward shift and increased variability of ENSO due to global warming have been identified and may have significant effects on extreme SSTs and SST variability within both regions within the tropical Atlantic [25]. As an additional mechanism by which all three CIs may affect US surface temperatures, high SST anomalies within the tropical Atlantic (i.e., a region limited to SSTs of 28.5°C or greater) have been found to generate convection over the Caribbean and anticyclonic circulation anomalies in the upper troposphere over the Gulf of Mexico and Great Plains, resulting in enhanced subsidence, reduced cloud cover, and higher surface warming for large parts of the US [26]. As such, these conditions were found to be associated with a higher frequency of heat waves for much of the US east of the Rocky Mountains.

CIs that characterize atmospheric patterns over portions of the northern Atlantic Ocean have also been found to have significant impacts on US weather and temperatures. The AO [27], for example, is a large-scale climate pattern that describes the strength of counterclockwise-circulating winds at approximately 55°N latitude. A belt of strong winds at this latitude strengthen during the positive phase of the AO, which results in colder air being confined to the polar regions. Warming during the positive phase of AO has been found to be especially significant over the eastern third of the US during the winter months of January to March [28]. The negative phase is represented by a weakening of the wind belt, which allows the colder air to penetrate southward into the midlatitudes. The NAO [29–30], which is closely linked with the AO, characterizes atmospheric pressure patterns over Greenland and those associated with the Subtropical High near the Azores. The positive phase of the NAO is linked to below-average pressures over Greenland and the North Atlantic and above-average pressure over the Azores as well as the eastern US and western Europe; opposite conditions are observed during the negative phase. Such pressure patterns tend to cause the eastern US to experience above average temperatures during strong positive phases of the NAO and below average

 doi:10.20944/preprints202306.1546.v1

temperatures during strong negative phases [31]. Volkov et al. [32] have also demonstrated that large-scale heat divergence throughout the North Atlantic resulting from these atmospheric patterns results affects the temperature of the Florida Current, which can also have some effect on land surface temperature along the East Coast of the US. A third CI, the Eastern Asia Western Russia index (EAWR) [28], also characterizes atmospheric pressure anomalies within the central North Atlantic as well in Europe, northern China, and near the Caspian Sea. Though previous studies regarding a potential connection between the EAWR and US land temperatures are sparse, there is evidence of a potential link with precipitation in portions of the US [33]; therefore, for the sake of completeness, the EAWR was considered in the current study.

Encompassing a large area of the North Atlantic that significantly overlaps regions that are characterized by the WHWP, NTA, TNA, NAO, and the EAWR, the AMO [34] provides a weighted average of SSTs from the Equator to approximately 70°N. Average SSTs in this region have been found to vary on a low-frequency multi-decadal time scale. Due to its potential contribution to the PDO [35] and overall influence on northern hemisphere surface temperatures [36], particularly over North America and Europe, the AMO represents yet another CI that must be considered in any study on the effects of climate variability on temperatures in the US.

Based on the discussion above, the present study consists of two parts. The first part attempts to link long-term average monthly mean, minimum, and maximum temperatures throughout the US to any one of a comprehensive set of CIs (see Table 1) in order to compare potential links between mean and extreme temperatures and the modes of climate variability represented by the CIs tested. The CIs considered include those characterizing atmospheric activity (i.e. pressure and height anomalies) and SSTs over and within portions of the central and northern Pacific and Atlantic Oceans and the Caribbean (see Figure 1 for approximate locations) and for which strong links to surface temperatures within the US have been previously identified or are plausible. The results would assist in identifying the existence of spatial patterns over which specific CIs exhibit a dominant link to long-term mean and/or extreme surface temperatures. Such information would contribute to a better understanding of the long-term variability in mean temperature as well the intensity and frequency of heat waves. The data and methodology used to assess these links are discussed in Section 2, while the results of the analyses are provided in Section 3. A discussion of how the final results fit or diverge from the narrative formed by previous studies as well as how they are or are not consistent with similar previous analyses related to precipitation and sea levels is provided in Section 4. Final concluding remarks are reserved for Section 5.

2. Materials and Methods

2.1. Data

Monthly time series of mean, minimum, and maximum surface temperature collected from 1948 to 2018 were obtained from the National Oceanographic and Atmospheric Administration (NOAA) United States Historical Climatology Network (USHCN) [37–38] database for sites located throughout the contiguous US; the study area and site locations are shown in Figure 2.

Mean values of monthly CI data were obtained from the NOAA Physical Sciences Laboratory (PSL) [22]. The current study considers numerous CIs (see Table 1 for the names and periods of record for each CI) characterizing regional atmospheric pressure or height anomalies and sea surface temperatures (SSTs) over and within the Atlantic and Pacific Oceans and Caribbean. Only CIs that characterize activity in or near regions where links to US surface temperatures have already been identified were considered. All CIs have similar periods of record to ensure consistency between the results.

2.2. Correlation Strength and Significance

The methodology used in the current study includes three major steps. The first step entailed collecting available monthly temperature data from the USGCN over the study period of January 1948 to December 2018 at the sites shown in Figure 2; data was collected from a total of 1,218 sites.

Preprints (www.preprints.org) | NOT PEER-REVIEWED | Posted: 21 June 2023 doi:10.20944/preprints202306.1546.v1

The data were then formatted into an input file that could be read and analyzed by the HydroMetriks Climate Tool (Hydro-CLIM) developed by Giovannettone [39].

The second step involved using Hydro-CLIM and an R-script to estimate the correlation strength and significance, respectively, between long-term average monthly mean, minimum, and maximum surface temperatures and the CIs listed in Table 1 for all sites. Similar to the analyses performed in Giovannettone et al. [40] and Giovannettone [33] with regard to monthly precipitation throughout North and South America, the correlation analysis itself consisted of three parts. The first part involved identifying three parameters required by Hydro-CLIM to perform the correlation analysis: sliding window size for long-term averaging, lag time between the temperature and CI sliding windows, and the beginning month of each temperature sliding window. Correlation strength

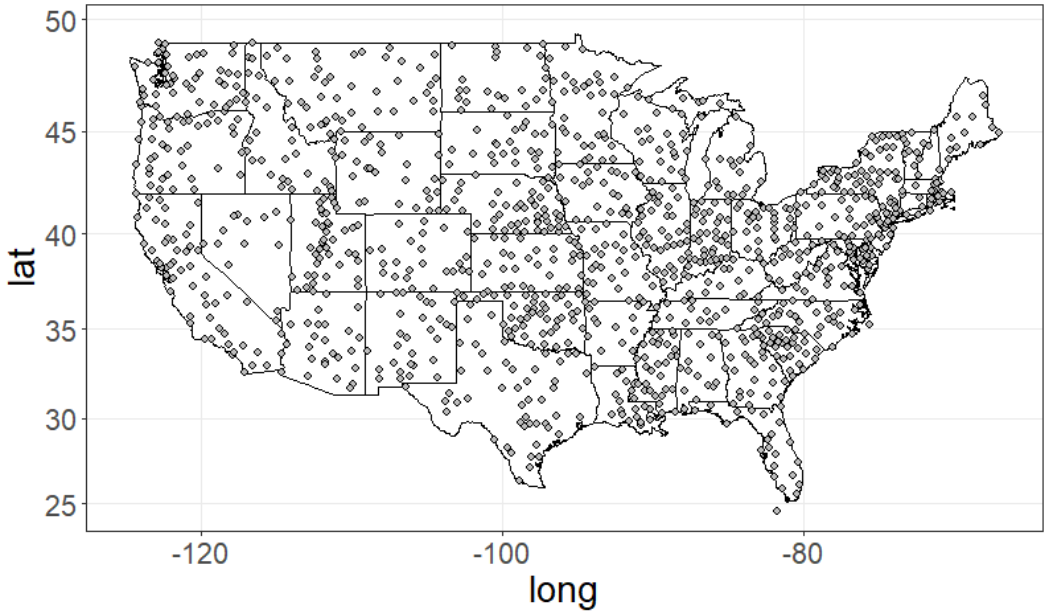

Figure 2. Locations of US Historical Climatology Network (USHCN) [37–38] temperature measurement stations used throughout the US.

(i.e., Pearson's r) between surface temperature and each CI was performed using sliding windows (SW) that ranged in size from 1 to 90 months using lag times (LT) ranging from 0 to 60 months. The mean temperature was then computed for all beginning months (BM = 1 to 12 (i.e., January to December)) using Equation (1):

$$\overline{ST_t} = \frac{1}{W} \sum_{BM}^{BM+W-1} ST_m, \qquad (1)$$

where $\overline{ST_t}$ is the average monthly mean, minimum, or maximum surface temperature computed for each sliding window defined by a beginning $m = BM$ of year t to an ending month of m=BM+W-1. Mean values of each CI were similarly calculated for all lag times (Equation (2)):

$$\overline{CI_t} = \frac{1}{W} \sum_{BM-LT}^{BM-LT+W-1} CI_m, \qquad (2)$$

with the major exception being that the computation window is set back a number of months compared to the monthly temperature window equal to the lag time (LT) being considered. As was done in Giovannettone [33], sites must have a minimum of eight valid pairs of long-term mean SL/CI data (i.e., no data values are missing over at least 8 sliding windows). The overall optimal sliding

Preprints (www.preprints.org) | NOT PEER-REVIEWED | Posted: 21 June 2023 doi:10.20944/preprints202306.1546.v1

window size and lag time between the temperature and CI sliding windows were then identified and applied to all sites analyzed and used to identify the third site-specific parameter (i.e., beginning month) that resulted in maximum correlation at each site. Following optimization of all three parameters, one dominant CI that resulted in the highest magnitude of linear correlation was identified at each site for each temperature dataset.

Since the potential effects of spurious and serial correlation on the results is a key concern in the type of analysis being performed, cross-validation and significance testing were performed on all correlation results. Initially, the Leave-One-Out Cross-Validation (LOOCV) technique [41] was used, after which the statistical significance of each correlation was estimated through a p-value that was computed using a bootstrap technique [42–43]. The correlation between surface temperatures and the dominant CI identified at each site for each temperature dataset was assumed to be strong and significant, and thus retained in the final results, if the Pearson's r value was greater than or equal to 0.60 and the p-value was less than or equal to 0.05 (i.e., rejection of the "no correlation" null hypothesis at the 95% confidence level).

The final step in the current analysis involved combining the temperature correlation results with similar results pertaining to precipitation and sea levels provided by Giovannettone [33] and Giovannettone et al. [44], respectively, in an attempt to identify consistent links between regional weather and climate, as well as sea levels, that would help focus future research on the impacts of climate variability in these areas. Maps that clearly illustrate consistencies as well as differences between the links identified were developed.

3. Results

3.1. Optimal Sliding Window Size and Lag Time

Preliminary correlation analyses were performed using a range of sliding window sizes and lag times. The results of these analyses helped identify specific CIs (WHWP and TSA) that exhibited widespread dominant signals; these CIs were used to identify a sliding window size over which mean, maximum, and minimum surface temperatures and CI values were averaged as well as a lag time between the surface temperature and CI sliding windows that resulted in maximum correlation. Figure 3 shows the correlation results for sliding window sizes ranging from 1 to 90 months using zero lag time and an optimal site-specific beginning month for only those sites at which either the WHWP (Figure 3a) or the TSA (Figure 3b) exhibited a dominant correlation with mean surface temperatures. As can be observed in Figure 3a, the correlation with the WHWP increases

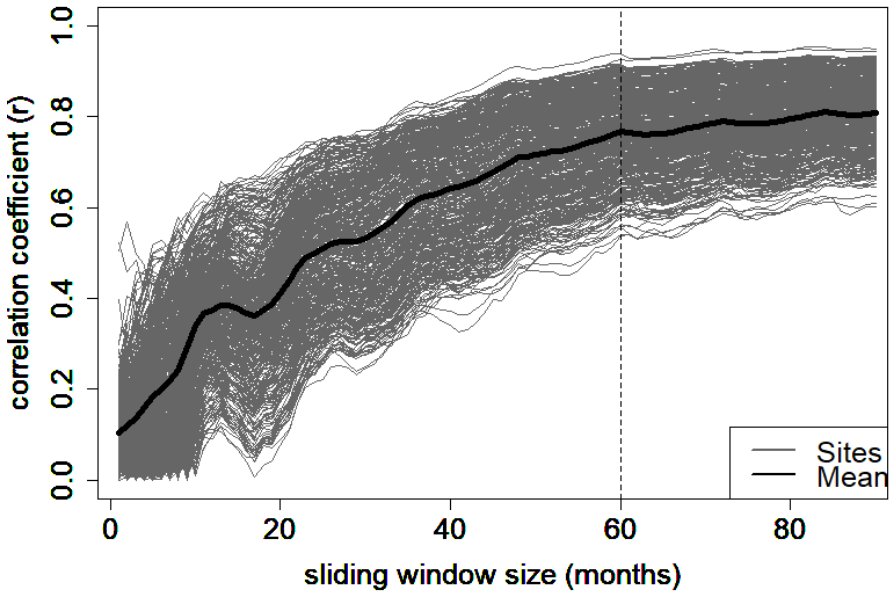

Preprints (www.preprints.org) | NOT PEER-REVIEWED | Posted: 21 June 2023 doi:10.20944/preprints202306.1546.v1

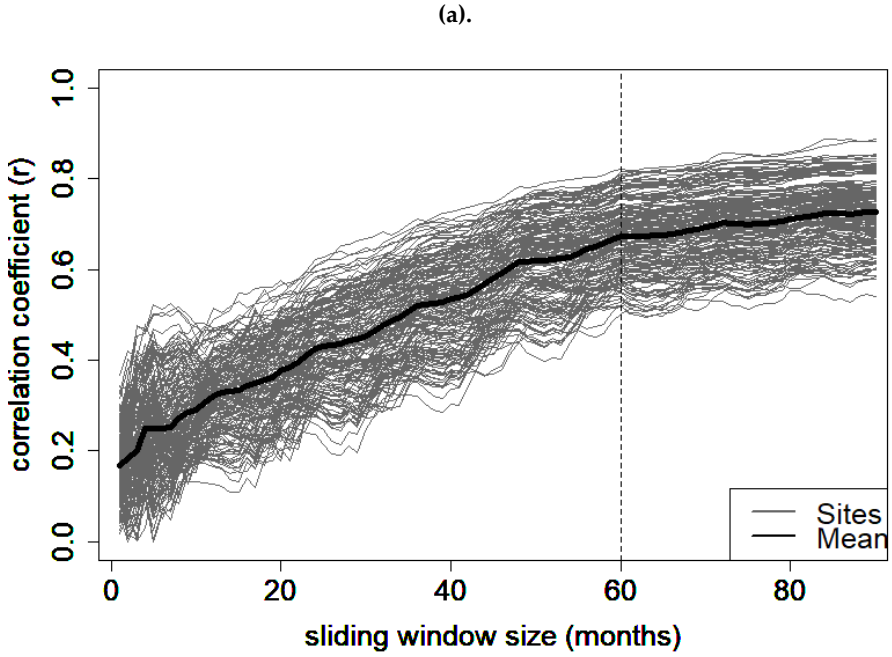

Figure 3. Resulting correlation magnitudes at sites throughout the US at which mean surface temperature correlates strongest with the (a) WHWP and (b) the TSA using sliding windows sizes ranging from 1 to 90 months and lag time = 0 months over the time period of 1948–2018. The dashed lines indicate the selected optimal sliding window size.

steadily between window sizes of 0 to a local maximum of 60 months, after which the improvement in correlation is minimal. Similar results can be seen in Figure 3b when considering the TSA. As a result of these findings and in order ensure consistency between all site correlation analyses, the sliding window size for all sites and surface temperature analyses was defined to be 60 months within the current study; this is consistent with the results from previous similar studies [39–40, 44].

Similar tests to those performed above with regard to sliding window size were also performed in an attempt to identify an optimal lag time that could be used for all site analyses. The range of lag times tested was 0 to 60 months using the previously identified optimal window size of 60 months. It should be noted that such a large window size, in addition to the fact that only averaging windows within which there are no missing values are considered within each correlation analysis, will result in the number of data points used in each analysis being reduced compared to if shorter sliding windows had been utilized. This issue is alleviated by the fact that the period of record used throughout (i.e., 1948–2018) allows a large number of data points to be available even following long-term averaging. Analysis using the range of lag times above was again

only performed for sites with which the WHWP and TSA exhibited dominant correlation with mean surface temperature. Correlation strength was not found to vary significantly over the range considered, though a slight peak was found at a lag time equal to 0 months (not shown). Therefore, in order to ensure consistent comparisons between all sites, a standard lag time of 0 months was used was all future correlation analyses within the current study.

3.2. Correlation Strength and Significance

After determining the sliding window size and lag time that resulted in overall optimal correlation, these parameters were used along with the site-specific optimal beginning month to identify the CI(s) that exhibited maximum correlation with long-term mean, maximum, and minimum surface temperatures at all sites over the period of record (1948-2018); a total of 1,218 sites were initially considered in each case. A wide range of correlation magnitudes were identified. Following cross-

Preprints (www.preprints.org) | NOT PEER-REVIEWED | Posted: 21 June 2023 doi:10.20944/preprints202306.1546.v1

validation, the percentage of sites at which the dominant correlation magnitude with respect to long-term monthly mean, minimum, and maximum temperatures was estimated to be |r| >= 0.60 was 80.0%, 86.7%, and 72.0%, respectively. Stronger correlations of at least |r| >= 0.80 were identified at 19.8%, 17.3%, and 16.1% of sites for the same temperature datasets, respectively. The spatial distributions of correlation magnitude and significance for long-term average mean, minimum, and maximum temperatures are shown in Figures 4a, 4b, and 4c, respectively. It can be seen that the strongest significant correlations were identified throughout much of the western half of the US and in the Northeast for all three datasets. An area extending southeast from the northern Great Plains to the southern East Coast exhibited weaker and less significant correlations than the rest of the US in all cases; in the case of mean and maximum temperatures, it can be seen that the weakest and least significant correlations were found in the northern and central Great Plains.

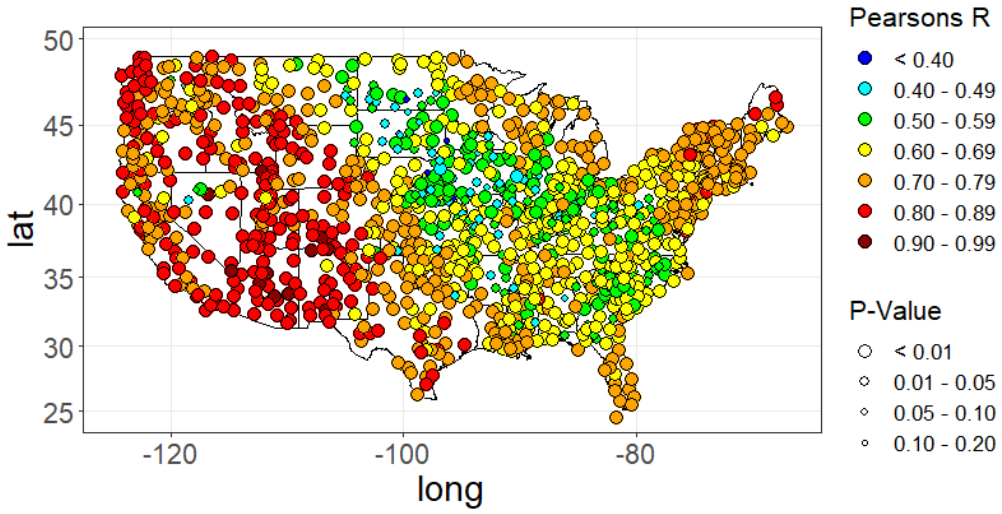

(a).

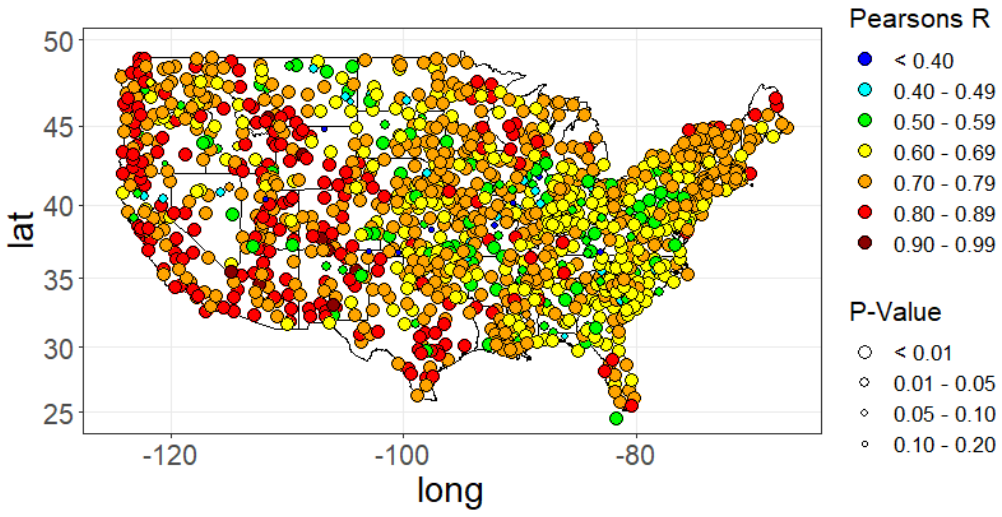

(b).

Preprints (www.preprints.org) | NOT PEER-REVIEWED | Posted: 21 June 2023 doi:10.20944/preprints202306.1546.v1

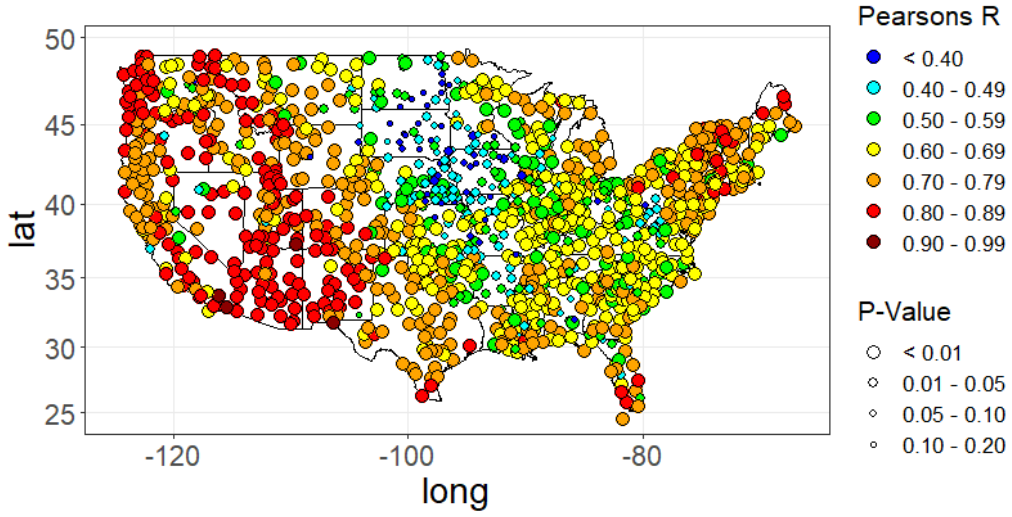

(c).

Figure 4. Results of correlation analyses using a sliding window size of 60 months and a lag time of 0 months; results are given in terms of correlation magnitude (|r|) and significance (p-value) for long-term average monthly (a) mean, (b) minimum, and (c) maximum surface temperatures. .

Sites exhibiting a correlation strength greater than a selected threshold of |r| >= 0.60 and a significance less than a selected threshold of p-value <= 0.05 were then retained to assess any spatial patterns that may exist with regard to the dominant CIs identified. Application of these conditions to the correlation analyses involving long-term average mean, minimum, and maximum surface temperatures resulted in 974 sites (80.0%), 1,050 sites (86.2%), and 876 sites (71.9%) being retained within each analysis, respectively. Lists of the CIs that exhibited dominance at a large majority of the sites for each analysis along with the percentage of sites at which they were found to be dominant are provided in Table 2. Refer to Figure 1 for the approximate locations characterized by each CI mentioned above.

Beginning with mean temperatures, the WHWP, AMO, and TSA exhibited the strongest significant links (see Columns 1 and 2 in Table 2) at the highest percentage of sites (45.8%, 16.6%, and 13.3% of sites where a dominant strong and significant correlation was identified, respectfully). The locations of these correlations as well as dominant correlations with the other CIs shown in the first two columns of Table 2 are illustrated in Figure 5a. Mean temperatures at sites throughout the western half of the US were predominantly linked to the WHWP, except for a thin strip of sites located along the West Coast that were more closely linked to NINO (as characterized by the CIs MEI, N3, N34, and N4). A dominant link with SSTs throughout the tropical North Atlantic as characterized by the AMO, NTA, TNA, and the EAWR can be observed throughout the southern Plains, the Appalachian Mountains, and the Northeast, while connections to Atlantic SSTs further north as characterized by the AO and NAO is observed along the southern East Coast as well as the portions of the Appalachian Mountains. Links associated with the NTA and TNA were reported as NTA/TNA due to the close proximity of both regions; links to the AO and NAO were reported as AO/NAO for the same reason. Finally, SSTs in the southern tropical Atlantic (i.e., TSA) were found to be the dominant link with mean surface temperatures through the northern Plains and the Midwest. The point should be made here that even though one dominant CI is shown for each site, multiple CIs were found to exhibit strong and significant correlations with temperatures at most sites. This means that if there are two or more CIs that exhibit similar correlation strengths, sites that are located nearby to each other may be characterized by dominant correlations with different CIs.

Preprints (www.preprints.org) | NOT PEER-REVIEWED | Posted: 21 June 2023 doi:10.20944/preprints202306.1546.v1

Table 2. Percentage of sites where CIs listed exhibit dominant strong and significant correlation with mean (Columns 1 & 2), minimum (Columns 3 & 4), and maximum (Columns 5 & 6) surface temperature using a sliding window size of 60 months and lag time = 0 over the period 1948–2018.

CI	% Sites	CI	% Sites	CI	% Sites
WHWP	45.8	**WHWP**	38.1	**WHWP**	31.4
AMO	16.6	**TSA**	28.1	**AMO**	27.4
TSA	13.3	**NINO**	11.0	**NTA/TNA**	11.4
NTA/TNA	11.2	**NTA/TNA**	8.6	**TSA**	8.7
NINO	6.1	**AMO**	5.5	**EAWR**	7.1
AO/NAO	2.5	**EAWR**	2.6	**NINO**	6.3
EAWR	2.3	**CAR**	2.4	**CAR**	4.2
CAR	1.4	**AO/NAO**	2.4	**AO/NAO**	1.8
PDO	0.4	**PDO**	0.9	**PDO**	0.8
Other	0.4	**Other**	0.5	**Other**	0.9

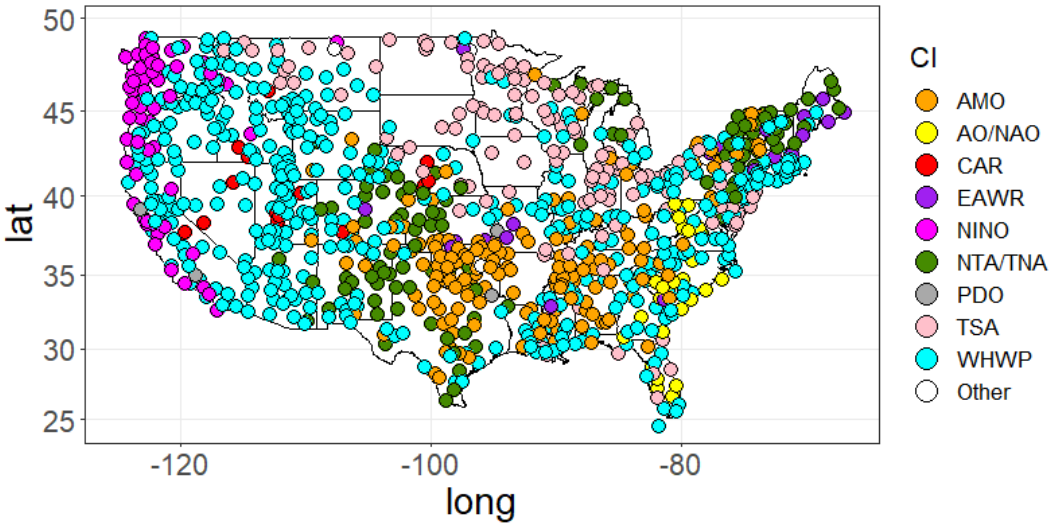

(a).

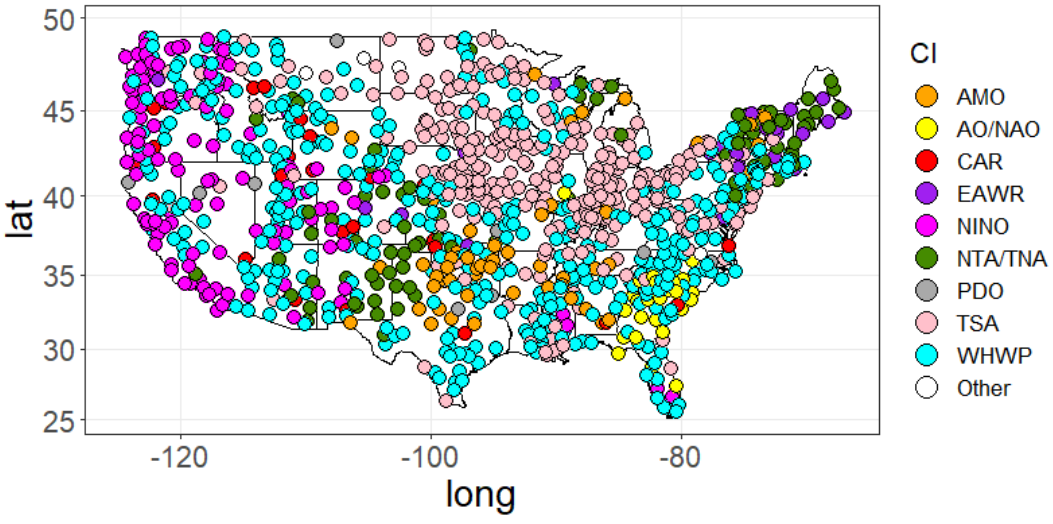

(b).

Preprints (www.preprints.org) | NOT PEER-REVIEWED | Posted: 21 June 2023 doi:10.20944/preprints202306.1546.v1

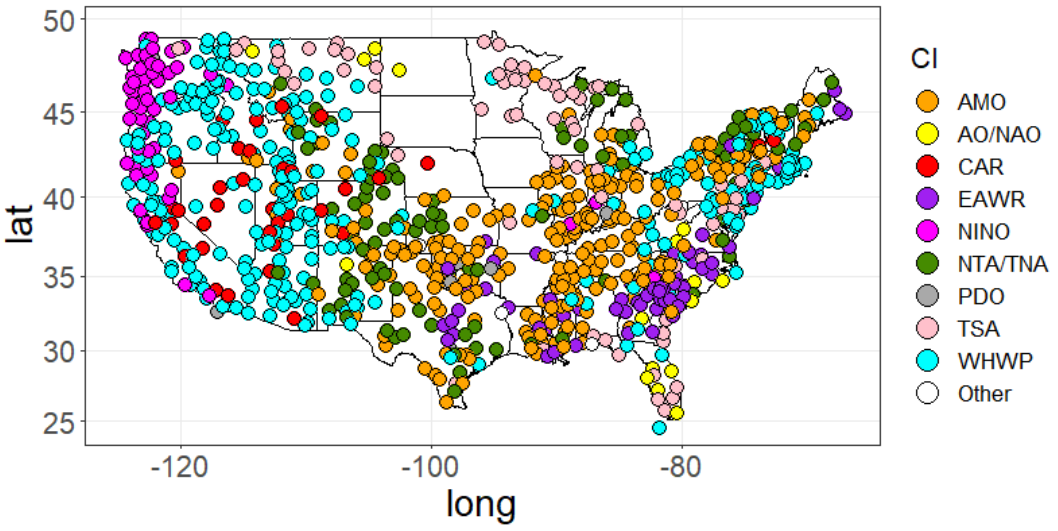

(c).

Figure 5. Spatial distributions of dominant CIs linked to (a) mean, (b) minimum, and (c) maximum monthly surface temperatures (window size = 60 months; lag = 0) for all sites at which |r| >= 0.60 and p <= 0.05 throughout the US during period 1948–2018. (See Table 1 for CI abbreviations.).

The CIs exhibiting dominant correlations with average long-term minimum surface temperature at the largest percentage of sites is similar to that found for average temperatures (see Columns 3 and 4 in Table 2) except for the fact that the dominance of the AMO was markedly less, while NINO (as characterized by the CIs MEI, N3, N34, N4, and the TNI) had a much larger spatial footprint. The WHWP remained the most dominant spatially at 38.1% of sites followed by the TSA at 28.1% and NINO at 11.0% of sites where a dominant strong and significant correlation was identified. The spatial distribution of said correlations as well as the dominant correlations with other CIs shown in Columns 3 and 4 of Table 2 is illustrated in Figure 5b. Average minimum surface temperatures at sites throughout the western half of the US were still predominantly linked to the WHWP, but there was a much stronger NINO presence that extended to the western edge of the Plains states. A dominant link with SSTs throughout the tropical North Atlantic as characterized by the AMO and NTA/TNA was contained to a much smaller area over the southern Plains than was observed for mean temperatures, while the same link in the Northeast was of relatively similar spatial extent. There was also a much more widespread link to the WHWP throughout the East Coast and Southeast than was seen in Figure 4a, though SSTs in the northern Atlantic (i.e., AO and NAO) retained a small portion of the southeastern coast. Finally, links to the TSA were much more pronounced and widespread throughout the northern and central Plains, Midwest, and the Ohio River Valley than was observed for mean temperatures.

The spatial distribution and extent to which the CIs mentioned above for mean and minimum temperatures was again similar when considering maximum surface temperatures except for a few key differences. The WHWP, AMO, and the NTA/TNA were found to be dominant at the greatest number of locations (namely at 31.4%, 27.4%, and 11.4% of sites where a strong and significant correlation was identified, respectively). The locations of these correlations as well as dominant correlations with the other CIs shown in Columns 5 and 6 of Table 2 are illustrated in Figure 5c. While maximum surface temperatures at sites throughout the western half of the US were again predominantly linked to the WHWP with a thin strip of sites located along the West Coast closely linked to NINO (as characterized by the CIs MEI, N12, N3, N34, N4, and the SOI), the CAR exhibited dominance at several western sites as well. The spatial extent of the link with tropical North Atlantic SSTs in the southern Plains was similar to that observed for mean temperatures, though the dominant correlation with the AMO extended much further east into the Tennessee and Ohio River Valleys as well as other portions of the Midwest. The dominance of the WHWP was much less pronounced

Preprints (www.preprints.org) | NOT PEER-REVIEWED | Posted: 21 June 2023 doi:10.20944/preprints202306.1546.v1

along the East Coast with the EAWR, AO, and NAO having a stronger presence in the Southeast as well as the AMO in the Northeast. Finally, dominant links with the TSA were much less common, especially in the northern Great Plains where it was difficult to identify any dominant correlations with maximum surface temperatures that were both strong and significant.

The results are consistent with those from previous studies with respect to the links between surface temperatures and ENSO along the West Coast and tropical Atlantic SSTs and temperatures in the Plains. Additional discussion on this as well as on findings that have not been revealed in prior studies is provided in Section 4.

4. Discussion

Correlation analyses between long-term monthly mean, maximum, and minimum surface temperatures and several climate indices (CIs) were performed over the period of record 1948–2018 in an attempt to identify spatially consistent links between various manifestations of climate variability and surface temperatures at sites located throughout the US. Analysis of long-term (60-month) averages of each temperature dataset revealed dominant links by a few prominent CIs: namely the ENSO CIs along the West Coast, the WHWP throughout the interior western half and a large portion of the eastern half of the US, the AMO in the southern Great Plains and Midwest, the NTA and TNA in the southern Great Plains and Northeast, the TSA throughout the northern Great Plains and Midwest, and the EAWR in the Southeast and Northeast. These results are consistent with mechanisms identified in the literature as described previously and serve as a basis from which to identify potential CIs that deserve additional research regarding their effect on weather in a particular region of the US.

The significant effect of SST variability within the Pacific Ocean and Gulf of Mexico on temperatures throughout the western half of the US is confirmed through the dominant correlations between long-term mean, maximum, and minimum temperatures and the CIs characterizing ENSO as well as the WHWP. The influence of ENSO's effect on Rossby waves from the west is especially obvious at sites located along the entire US West Coast where ENSO is most dominant.

The dominant influence of SSTs either directly to the west or south declines significantly slightly as one moves slightly east of the Rocky Mountains into the Great Plains. A strong link to the AMO manifests itself for all temperature datasets within the southern Plains. This AMO region expands to the east when considering mean temperatures and further expands to the northeast when assessing the AMO's potential link to monthly maximum temperatures. The dominant link of northern (in this case tropical northern) Atlantic SSTs to all temperature types in the southern Plains is further confirmed by the added dominance of the NTA/TNA on the western border with the Rocky Mountains. In contrast, the northern Great Plains is dominated by the TSA for all temperature types, though the significant of these links progressively decreases moving from minimum to mean and on to maximum monthly surface temperatures. Both links to the tropical Atlantic SSTs (and potentially to the AMO, though the AMO covers a much larger area that extends far north of the tropics), particularly in the case of maximum temperatures, supports prior research that has shown a significant effect of tropical Atlantic SSTs on the incidence of heat waves throughout the Great Plains [26], though it is interesting to note that the current suggest that this influence may extend much further to the east and northeast.

Dominant links associated with atmospheric behavior over north of the tropical Atlantic was limited the Southeast and portions of the mid-Atlantic as well as the extreme Northeast when considering all temperature types. Links with the AO and NAO were present in the Southeast and within a small area near the Shenandoah Valley in all cases as was a link between the EAWR and temperatures in the extreme Northeast. When considering monthly maximum temperatures, a strong link with the EAWR also manifested itself over a large portion of the Southeast that included the states of Georgia and North and South Carolina. Such links are supported by prior studies previously mentioned [28–30, 32], especially proximity to the coast.

Based on the results of the current study with regard to surface temperature, Figure 6a provides a clearer, but more general, representation of approximate regions over which the CIs mentioned

Preprints (www.preprints.org) | NOT PEER-REVIEWED | Posted: 21 June 2023 doi:10.20944/preprints202306.1546.v1

above were dominant. The regions as shown do not depict the more detailed differences observed between long-term mean, minimum, and maximum monthly temperatures, but merely provide an overall assessment in order to guide future research and as a way to compare to similar analyses performed in prior studies. To this end, Figures 6b and 6c present similar maps that provide general assessments of results from prior studies focusing on long-term monthly precipitation [33] and sea levels [44], respectively. One key difference that should be noted here is that due to the shorter period of record over which data on the Madden-Julian Oscillation (MJO) is available, the MJO was not considered in the current study; as a result, comparisons with between Figures 6a and 6b for the western half of the US cannot be made based on the results presented, though additional results in Giovannettone [33] did indicate a strong link to ENSO when longer lag times were considered, which is consistent with some of the findings here and in Giovannettone et al. [44], though no lag times were used in both instances.

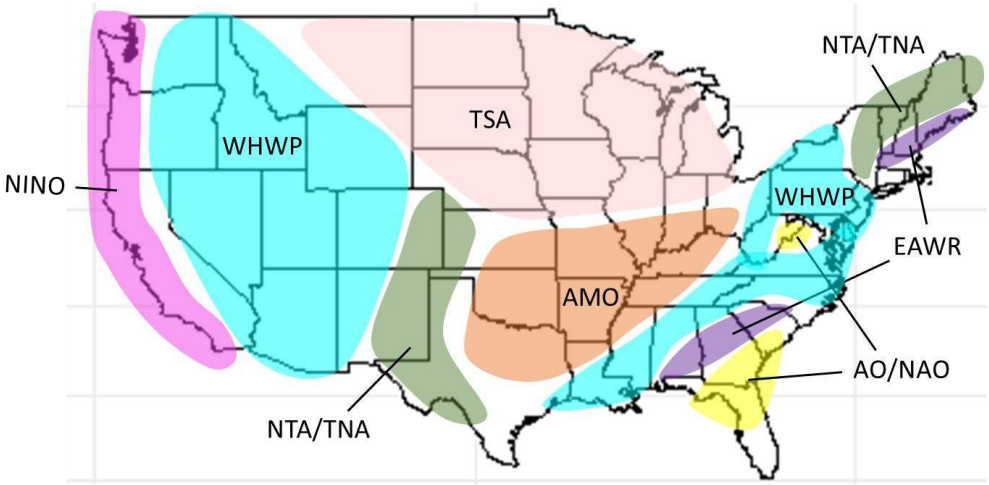

(a).

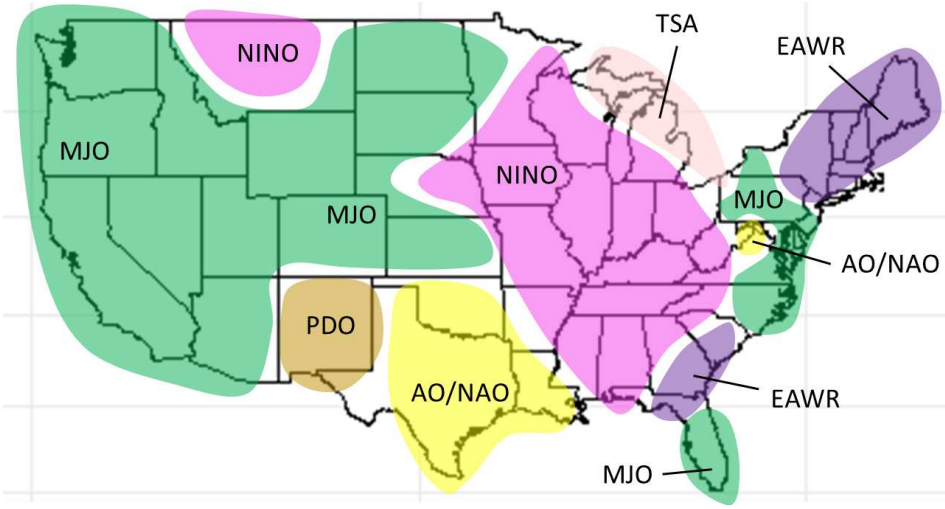

(b).

Preprints (www.preprints.org) | NOT PEER-REVIEWED | Posted: 21 June 2023 doi:10.20944/preprints202306.1546.v1

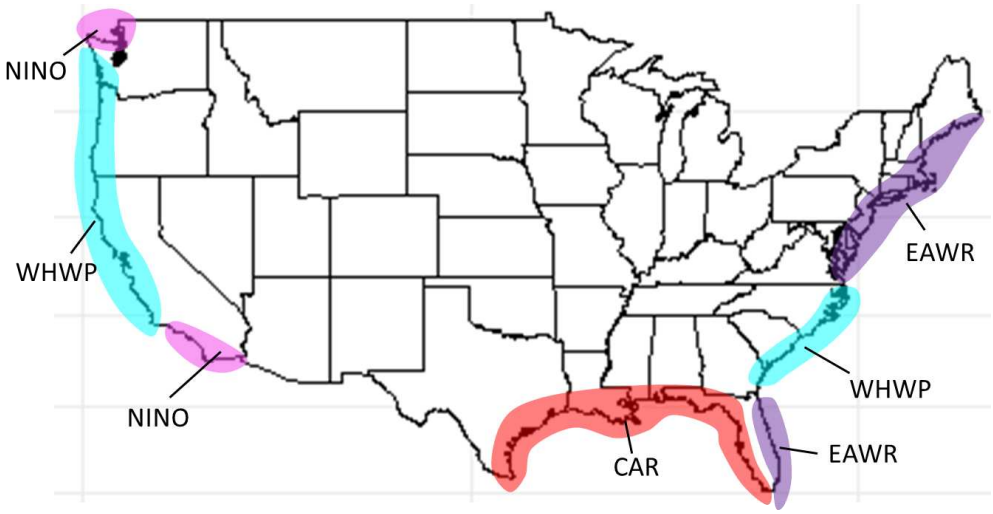

(c).

Figure 6. Spatial distributions of strong and significant (|r| >= 0.60 and p <= 0.05) correlations identified between the dominant CIs indicated and long-term (a) surface temperature, (b) precipitation, and sea levels using optimal lag times and beginning months as described (a) within the current study as well as (b) and (c), respectively. (See Table 1 for CI abbreviations.).

Unlike in the western half of the US, some informed comparisons can be made throughout the eastern half. The apparent links between atmospheric behavior over the northern Atlantic (i.e., AO/NAO and EAWR) and weather over the Northeast, the Shenandoah Valley, and a large portion of the Southeast is evident for both temperature and precipitation. Further evidence of potential teleconnections with the EAWR are evident in the fact that it represented the dominant CI with regard to long-term mean sea levels along both the Northeast and Southeast coastlines (Figure 6c). These results suggest that this potential weather and sea level connection to the EAWR should be studied in further detail as literature on this topic is extremely sparse if not nonexistent. The EAWR also presents an opportunity to identify teleconnections between weather in parts of the US and weather in other regions characterized by the EAWR (i.e., Caspian Sea, Europe, and northern China).

5. Conclusions

There is a lack of knowledge and data to identify communities and locations most at risk from extreme temperatures, particularly with respect to extended period of high temperatures (i.e., heat waves), which can have detrimental effects on human health and the natural and built environments. Such knowledge is crucial to make planning decisions related to decreasing vulnerability and increasing resilience both now and in the future, particularly in the face of climate change. Due to the direct projected effects of climate change on mean and extreme temperatures, it is essential to be aware of the underlying mechanisms related to climate variability that can be linked to short- and long-term fluctuations in temperatures, on top of which the projected effects of climate change can be superimposed.

In an attempt to understand some of the underlying mechanisms related to long-term temperature variability, potential links between several climate indices (CIs) and long-term average mean, minimum, and maximum surface temperatures were assessed during the study period 1948–2018. The CIs considered in the current study either characterized SSTs over portions of the eastern Pacific Ocean, the tropical Atlantic Ocean, and the Gulf of Mexico and Caribbean, or atmospheric behavior in terms of height and pressure anomalies over the northern Atlantic Ocean. It was found that the Western Hemisphere Warm Pool (WHWP), which characterized SSTs south of the US, exhibited the most widespread dominant link with mean and extreme temperatures throughout the western US and portions of the East. Dominant links with ENSO were also identified, though these were limited

to a thin region extending along the entire West Coast. Dominant links to SSTs southeast of the US (as characterized by the AMO, NTA, TNA, and TSA) within the northern and southern tropical Atlantic Ocean were found in all cases throughout the northern and southern Great Plains as well as the Great Lakes regions. Temperatures within large portions of the Northeast and Southeast were linked to changes in atmospheric patterns over the northern Atlantic as characterized by the AO, NAO, and EAWR. This is not surprising as the locations of atmospheric conditions characterized three CIs are adjacent to each other, though previous research has focused on the AO and NAO while devoting little attention to the EAWR. Proposed ideas with regard to potential mechanisms were proposed, but additional research is required to confirm the level of causality regarding all links that were identified.

The results from the current study were then compared to similar results from previous studies that were focused on long-term precipitation and sea levels in order to determine the extent to which similar links were found. The dominance of the WHWP and ENSO in the West was shared by the temperature and sea level analyses, while the MJO revealed stronger links with precipitation. An additional similarity that was found was the dominance of the EAWR in the Northeast for both weather parameters as well as long-term sea levels. These results, as well as the current lack of research related to any effects of the EAWR on weather and climate in the US, stress the need for future research focused in this area.

Funding: This research was not funded.

Informed Consent Statement: Not applicable.

Data Availability Statement: The data (climate index and surface temperature datasets) used in this study are publicly available at [22] and [37], respectively.

Acknowledgments: The authors would like to acknowledge the International Center for Integrated Water Resources Management (ICI-WaRM) for facilitating the development of the ICI-WaRM Regional Analysis of Frequency Tool (ICI-RAFT) (https://www.iwr.usace.army.mil/Missions/Hydrology/ICI-RAFT-ICIWaRM-Regional-Analysis-of-Frequency-T/), which inspired and was used to validate the development and accuracy, respectively, of Hydro-CLIM.

Conflicts of Interest: The authors declare no conflicts of interest.

References

1. IPCC (Intergovernmental Panel on Climate Change). Summary for Policymakers. In: *Climate Change 2021: The Physical Science Basis. Contribution of Working Group I to the Sixth Assessment Report of the Intergovernmental Panel on Climate Change*; Masson-Delmotte, V., Zhai, P., Pirani, A., Connors, S.L., Péan, C., Berger, S., Caud, N., Chen, Y., Goldfarb, L., Gomis, M.I., Huang, M., Leitzell, K., Lonnoy, E., Matthews, J.B.R., Maycock, T.K., Waterfield, T., Yelekçi, O., Yu, R., Zhou, B., Eds.; Cambridge University Press: Cambridge, United Kingdom, and New York, NY, USA, 2021; pp. 3–32.
2. Lee, J.-Y.; Marotzke, J.; Bala, G.; Cao, L.; Corti, S.; Dunne, J.P.; Engelbrecht, F.; Fischer, E.; Fyfe, J.C.; Jones, C.; Maycock, A.; Mutemi, J.; Ndiaye, O.; Panickal, S.; Zhou, T. Future Global Climate: Scenario-Based Projections and Near-Term Information. In: *Climate Change 2021: The Physical Science Basis. Contribution of Working Group I to the Sixth Assessment Report of the Intergovernmental Panel on Climate Change*; Masson-Delmotte, V., Zhai, P., Pirani, A., Connors, S.L., Péan, C., Berger, S., Caud, N., Chen, Y., Goldfarb, L., Gomis, M.I., Huang, M., Leitzell, K., Lonnoy, E., Matthews, J.B.R., Maycock, T.K., Waterfield, T., Yelekçi, O., Yu, R., Zhou, B., Eds; Cambridge University Press: Cambridge, United Kingdom, and New York, NY, USA, 2021; pp. 553–672.
3. Perkins, S.E. A review on the scientific understanding of heatwaves—their measurement, driving mechanisms, and changes at the global scale." *Atmos. Res.* **2015**, 164, 242–267.
4. Gershunov, A.; Guirguis, K. California heat waves in the present and future. *Geophys. Res. Lett.* **2012**, 39, L18710.
5. Keellings, D.; Moradkhani, H. Spatiotemporal Evolution of Heat Wave Severity and Coverage Across the United States. *Geophys. Res. Lett.* **2020**, 47, e2020GL087097.

6. Raei, E.; Nikoo, M.R.; AghaKouchak, A.; Mazdiyasni, O.; Sadegh, M. GHWR, A multi-method global heatwave and warm-spell record and toolbox. *Sci. Data* **2018**, 119, 188–196.
7. Zhang, Y.; Ayyub, B. Projecting heat waves temporally and spatially for local adaptations in a changing climate: Washington D.C. as a case study. *Nat. Hazards* **2020**, 103, 731–750.
8. Vose, R.S.; Easterling, D.R.; Kunkel, K.E.; LeGrande, A.N.; Wehner, M.F. 2017. Temperature Changes in the United States. In: *Climate Science Special Report: Fourth National Climate Assessment, Volume I*; Wuebbles, D.J., Fahey, D.W., Hibbard, K.A., Dokken, D.J., Stewart, B.C., Maycock, T.K., Eds.; US Global Change Research Program (USGCRP), Washington, D.C., USA, 2017; pp. 185–206.
9. van der Weil, K.; Bintanja, R. Contribution of climatic changes in mean and variability to monthly temperature and precipitation extremes. *Commun. Earth Environ.* **2021**, 2, 1.
10. Wallace, J.M.; Rasmusson, E.M.; Mitchell, T.P.; Kousky, V.E.; Sarachik, E.S.; von Storch, H. J. On the structure and evolution of ENSO-related climate variability in the tropical Pacific: Lessons from TOGA. *Geophys. Res.* **1998**, 103, 14241–14259.
11. Martineau, P.; Nakamura, H.; Kosaka, Y. Influence of ENSO on North American subseasonal surface air temperature variability. *Weather Clim. Dyn.* **2021**, 2, 395–412.
12. Halpert, M.S.; Ropelewski, C.F. Surface temperature patterns associated with the Southern Oscillation. *J. Clim.* **1992**, 5, 577–593.
13. Ropelewski, C.F.; Halpert, M.S. North American precipitation and temperature patterns associated with the El Niño-Southern Oscillation (ENSO). *Mon. Weather Rev.* **1986**, 114, 2352–2362.
14. Wolter, K.; Timlin, M.S. Monitoring ENSO in COADS with a seasonally adjusted principal component index. In Proceedings of the 17th Climate Diagnostics Workshop, Norman, OK, USA, 18–23 October 1992; pp. 52–57.
15. Ropelewski, C.F.; Jones, P.D. An extension of the Tahiti-Darwin Southern Oscillation Index. *Mon. Weather Rev.* **1987**, 115, 2161–2165.
16. Trenberth, K.E.; Stepaniak, D.P. Indices of El Niño evolution. *J. Clim.* **2001**, 14, 1697–1701.
17. Mantua, N.J.; Hare, S.R. The Pacific Decadal Oscillation. *J. Oceanogr.* 2002, 58, 35–44.
18. Wang, C.; Enfield, D.B. The Tropical Western Hemisphere Warm Pool. *Geophys. Res. Lett.* **2001**, 28, 1635–1638.
19. Misra, V.; Groenen, D.; Bhardwaj, A.; Mishra, A. The warm pool variability of the tropical northeast Pacific. *Int. J. Climatol.* **2016**, 36, 4625–4637.
20. Enfield, D.B.; Lee, S.K.; Wang, C. How are large western hemisphere warm pools formed? *Prog. Oceanogr.* **2006**, 70, 346–365.
21. Penland, C.; Matrosova, L. Prediction of tropical Atlantic sea surface temperatures using Linear Inverse Modeling. *J. Clim.* **1998**, 11, 483–496.
22. Enfield, D.B.; Mestas, A.M.; Mayer, D.A.; Cid-Serrano, L. How ubiquitous is the dipole relationship in tropical Atlantic sea surface temperatures? *J. Geophys. Res. Oceans* **1999**, 104, 7841–7848.
23. Jiang, L.; Li, T. Relative roles of El Niño-induced extratropical and tropical forcing in generating Tropical North Atlantic (TNA) SST anomaly. *Clim. Dyn.* **2019**, 53, 3791–3804.
24. Yang, Y.; Wu, L; Guo, Y.; Gan, B.; Cai, W.; Huang, G.; Li, X.; Geng, T.; Jing, Z.; Li, S.; Liang, X.; Xie, S.P. Greenhouse warming intensifies north tropical Atlantic climate variability. *Sci. Adv.* **2021**, 7, eabg9690.
25. Lopez, H.; Kim, D.; West, R.; Kirtman, B. Modulation of North American Heat Waves by the Tropical Atlantic Warm Pool. *J. Geophys. Res. Atmos.* **2022**, 127, e2022JD037705.
26. Thompson, D.W.J.; Wallace, J.M. The Arctic oscillation signature in the wintertime geopotential height and temperature fields. *Geophys. Res. Lett*. **1998**, 25, 1297–1300.
27. Higgins, R.W.; Leetmaa, A.; Xue, Y.; Barnston, A. Dominant factors influencing the seasonal predictability of U.S. precipitation and surface air temperature. *J. Clim.* **2000**, 13, 3994–4017.
28. Barnston, A.G.; Livezey, R.E. Classification, seasonality and persistence of low frequency atmospheric circulation patterns. *Mon. Weather Rev.* **1987**, 115, 1083–1126.
29. Hurrell, J.W. Decadal Trends in the North Atlantic Oscillation: Regional Temperatures and Precipitation. *Science* **1995**, 269, 676–679.
30. Iles, C.; Hegerl, G. Role of the North Atlantic Oscillation in decadal temperature trends. *Environ. Res. Lett.* **2017**, 12, 114010.
31. Volkov, D.L.; Baringer, M.; Smeed, D.; Johns, W.; Landerer, F.W. Teleconnection between the Atlantic Meridional Overturning Circulation and sea level in the Mediterranean Sea. *J. Clim.* **2019**, 32, 935–955.

32. Giovannettone, J.P. Assessing the relationship between low-frequency oscillations of global hydro-climate indices and long-term precipitation throughout the United States. *JAMC* **2021**, 60, 87–101.
33. Enfield, D.B.; Mestas-Nuñez, A.M.; Trimble, P.J. The Atlantic multidecadal oscillation and its relation to rainfall and river flows in the continental U.S. *Geophys. Res. Lett.* **2001**, 28, 2077–2080.
34. Zhang, R.; Delworth, T.L. Impact of the Atlantic Multidecadal Oscillation on North Pacific climate variability. *Geophys. Res. Lett.* **2007**, 34, L23708.
35. Semenov, V.A.; Latif, M.; Dommenget, D.; Keenlyside, N.S.; Strehz, A.; Martin, T.; Park, W. The Impact of North Atlantic–Arctic Multidecadal Variability on Northern Hemisphere Surface Air Temperature. *J. Clim.* **2000**, 23, 5668–5677.
36. NOAA (National Oceanographic and Atmospheric Administration): U.S. Historical Climatology Network Monthly (USHCN) Version 2.5.5. Available online: https://www.ncei.noaa.gov/pub/data/ushcn/v2.5/ (Accessed 1 March, 2023)
37. Menne, M.J.; Williams, C.N.; Vose, R.S. The United States Historical Climatology Network monthly temperature data, Version 2. *BAMS* **2009**, 90, 993–1007.
38. NOAA (National Oceanographic and Atmospheric Administration): Climate indices: Monthly atmospheric and ocean time series. Available online: https://psl.noaa.gov/data/climateindices/list/ (accessed on 16 February, 2016)
39. Giovannettone, J.P. *HydroMetriks – Climate Tool (Hydro-CLIM)*. HydroMetriks, LLC: Silver Spring, MD, USA, 2020.
40. Giovannettone, J.P.; Paredes-Trejo, F.; Barbosa, H.; dos Santos, C.A.C.; Kumar, T.V.L. Characterization of links between hydro-climate indices and long-term precipitation in Brazil using correlation analysis. *Int. J. Climatol.* **2020**, 40, 5527–5541.
41. Efron, B. Estimating the error rate of a prediction rule: improvement on cross-validation. *JASA* **1983**, 78, 316–331.
42. Efron, B. Bootstrap methods: Another look at the jackknife. *Ann. Stat.* **1979**, 7, 1–26.
43. Enfield, D.B.; Mestas-Nuñez, A.M.; Trimble, P.J. The Atlantic multidecadal oscillation and its relation to rainfall and river flows in the continental U.S. *Geophys. Res. Lett.* **2001**, 28, 2077–2080.
44. Giovannettone, J.; Paredes-Trejo, F.; Amaro, V.E.; dos Santos, C.A.C. Assessing potential links between climate variability and sea levels along the coasts of North America. *Climate* **2023**, 11, 80.